Desalination and Water Treatment
www.deswater.com
doi: 10.5004/dwt.2022.28870

273 (2022) 149–161
October

A low-cost adsorbent deriving from eggshell modified with Mg(II)-doped hydroxyapatite for removal of Cd^{2+} from water

Xiangyi Gong[a,b,c,*], Dekang Meng[a,b,c], Zhang Peng[a], Zeya Wang[a], Dajun Ren[a], Fengying Wu[a]

[a]*School of Resource and Environmental Engineering, Wuhan University of Science and Technology, Wuhan 430081, China, emails: gxywust@163.com (X. Gong), 295944628@qq.com (D. Meng), pengzhang1995@163.com (Z. Peng), 13507282990@139.com (Z. Wang), dj_ren@163.com (D. Ren), 18389585372@163.com (F. Wu)*
[b]*Hubei Key Laboratory for Efficient Utilization and Agglomeration of Metallurgic Mineral Resources, Wuhan University of Science and Technology, Wuhan 430081, China*
[c]*Hubei Key Laboratory of Mine Environmental Pollution Control and Remediation, Hubei Polytechnic University, Huangshi 435003, China*

Received 4 May 2022; Accepted 21 August 2022

ABSTRACT

The industrial by-product cadmium can pollute the environment and be harmful to humans after being discharged from wastewater. In this study, a low-cost adsorbent deriving from kitchen waste eggshells (BC), was modified by magnesium-doped hydroxyapatite in order to form a new adsorbent (MHBC) capable of removing Cd^{2+} from water. When compared to BC, the adsorption capacity of MHBC was found to be greatly improved, while their equilibrium adsorption capacities were 4.82 and 49.41 $mg \cdot g^{-1}$, respectively. Kinetic, isothermal, and environmental factors' analyses suggested that chemisorption played a major role in the Cd^{2+} adsorption process delivered by MHBC. Particularly, chemical complexation, ion exchange, and electrostatic interaction could be the main mechanisms involved. Both the pseudo-second-order kinetics equation and the Sips isotherm model were found to fit the adsorption process well. Sips model revealed that the maximum adsorption capacity of MHBC at 25°C was 68.898 $mg \cdot g^{-1}$. Acidic conditions and the presence of Mg^{2+}, Pb^{2+}, Cu^{2+}, and Zn^{2+} were found to reduce the adsorption capacity of MHBC for Cd^{2+}. After three cycles, the removal percentage of Cd^{2+} by MHBC was still able to reach 78.75%. Therefore, our study suggests that MHBC is a highly efficient, green, and sustainable Cd^{2+}-removing adsorbent.

Keywords: Eggshell; Low-cost adsorbent; Hydroxyapatite; Cadmium

1. Introduction

The heavy metal cadmium in industrial wastewater can seep into soil and be absorbed by crops and human bodies, thereby causing a series of health problems, such as liver and kidney injury [1], reproductive system disorders [2], and cancer [3]. Therefore, it is necessary to find a simple and efficient method to remove cadmium from sewage. To date, many methods have been used in order to heavy metals from wastewater, including chemical precipitation [4], ion exchange [5], solvent extraction [6], membrane filtration [7], and electrochemical treatment [8]. However, these methods have some disadvantages such as incomplete removal, high operating cost, high energy consumption and secondary pollution [9]. Adsorption is the most commonly used method, thanks to its simple process, simple operation and high efficiency [10]. However,

* Corresponding author.

most of the adsorbents still have the problems of low efficiency, poor reuse performance and high cost. Low-cost modified adsorbents can effectively solve these problems due to their effectiveness, practicality, and widely available sources. The raw materials of the low-cost adsorbent can be agricultural and forestry wastes, animal manure, activated sludge and/or other materials rich in organic matter. During the past decade, biological wastes from the agricultural and the food industries (including bagasse, orange peel, watermelon peel, coconut shells and rice husks) have been used as potential biosorbents in an attempt to remove cadmium from water [11–15]. As a form of low-cost adsorbent, activated carbon has also been widely used in order to remove pollutants from wastewater [16,17].

Eggshell is one of the most common kitchen wastes. Approximately 65.5 million tons of eggs are produced worldwide each year. Eggshell is rarely used to produce adsorbents compared to lignin-containing biomass, and it has a composition of 94% calcium carbonate, 1% magnesium carbonate, 1% calcium phosphate and 4% organic matter [18]. In reality, the availability of eggshells should not be underestimated. Eggshells can be used as low-cost adsorbents capable of removing environmental contaminants after a high temperature pyrolysis that is similar to that employed for the preparation of biochar [19,20]. Furthermore, its adsorption performance can still be improved by a modification or a composition with other materials. Hydroxyapatite (HAP) is an important phosphorous mineral in nature and the main component of human bones and teeth [21]. HAP is widely used in soil remediation, water pollution treatment, medicine, and biology [22–24]. It causes little environmental pollution, and it is an environmentally friendly material. Moreover, HAP can adsorb heavy metal ions and some organic pollutants due to its special crystal structure [25,26]. The metal cation position occupied by the calcium ion in the HAP structure has a good reactivity, and can be substituted with other cations so as to generate different types of HAP. For example, Li uses Fe(II) as a doping ion in order to replace part of the Ca(II) for a HAP-doping modification experiment [27]. It was found that when the Ca:Fe ratio is 1:1, its adsorption capacity of Pb(II) was 1.8 times higher than that of ordinary HAP. Mg^{2+} have similar properties to Ca^{2+}, and studies have shown that HAP doped with Mg^{2+} can effectively remove lead ions from water [28].

After considering the aforementioned characteristics of the low-cost adsorbent and the pollution caused by cadmium-containing wastewater, the original eggshell adsorbent was, herein, firstly prepared by using the preparation method of biochar. Subsequently, not only HAP was combined with the eggshell adsorbent, but also Ca^{2+} was substituted by Mg^{2+} in the HAP in order to obtain a new low-cost adsorbent (MHBC). The characteristics and the mechanism of Cd^{2+} adsorption by MHBC were analyzed by physical and chemical characterization methods, kinetics, and isothermal adsorption experiments. The influence of pH, dosage, ionic strength, concomitant ions, and the initial Cd^{2+} concentration on the adsorption of Cd^{2+} by MHBC were investigated. Finally, the MHBC's regeneration performance was explored through the undertaking of repeated adsorption and desorption experiments.

2. Materials and methods

2.1. Reagents and materials

Chicken eggshells were obtained from Wuhan, Hubei. NaOH, $CdCl_2·2.5H_2O$, HNO_3, NaCl, $MgCl_2$, Na_2CO_3, Na_2SO_4, $Na_3PO_4·12H_2O$, $NaNO_3$, $Mg(NO_3)_2·6H_2O$, $Pb(NO_3)_2$, $Cu(NO_3)_2·3H_2O$, $Zn(NO_3)_2·6H_2O$, $(NH_4)_2HPO_4$, $NH_3·H_2O$ were purchased from Sinopharm Chemical Reagent Co., Ltd.

2.2. Adsorbent preparation and characterization

After the inner lining was removed, the eggshells were ground with a mortar to 100 meshes. They were then calcined in a tube furnace with nitrogen flow. The temperature rose to 500°C at a rate of 5°C per min and then continued for 2 h. After cooling to room temperature, the material was removed and stored under dry conditions. The obtained sample was named "BC".

HAP was prepared by hydration with $CaCl_2$ as a calcium source and with $(NH_4)_2HPO_4$ as a phosphorus source. Subsequently, 100 mL of a 1 mol·L^{-1} $(NH_4)_2HPO_4$ solution were added to 100 mL of a 1 mol·L^{-1} $CaCl_2$ solution at a constant rate under agitation, thereby ensuring that the value of the Ca/P (mole ratio) was 1.667. Following this step, 16 g of BC and ammonia were added to the mixture until the pH value reached 10 under magnetic stirring. The mixture was stirred for another 2 h. After sitting for 24 h, the gray products were washed with deionized water until its pH is 7. "HBC" was obtained after drying at 80°C overnight. Similarly, when the Mg doping was carried out, $MgCl_2$ was used as the magnesium source in order to ensure that the (Ca + Mg)/P = 1.667, repeating the above steps so as to obtain "MHBC" [28].

The main surface functional group characteristics of the adsorbents before and after modification were measured by Fourier Transform Infrared Spectroscopy (FTIR; Thermo Scientific Nicolet 6700; Thermo Fisher Scientific, USA). The surface morphology and the structure of the samples before and after the modification were measured by scanning electron microscopy (Apreo S HiVac; Thermo Fisher Scientific, USA; TESCAN MIRA LMS; TESCAN, Czech Republic). Characteristics of the specific surface area and pore structure were measured by fully automatic specific surface and porosity analyzer (ASAP 2460; Micro Instruments, USA). The X-ray diffraction (XRD) analysis was conducted in order to identify the crystallographic structures of the samples by using an X-ray diffractometer (Bruker D8 advance; Bruker, Germany). The zeta potential was measured with a zeta potential analyzer (Zetasizer Nano ZS90; Malvern, UK).

2.3. Adsorption experiments

Prior to the absorption experiments, 0.05 g of the adsorbent (BC, HBC, or MHBC) and 50 mL of the Cd^{2+} solution were added into a 100 mL conical flask. The flask was then shaken on a thermostatic oscillator at 200 rpm and 25°C. The adsorption kinetics experiments regarding the BC were conducted within 1440 min (15, 30, 60, 90, 120, 240, 360, 480, 600, 720, 840, and 1440 min), while those regarding the HBC and the MHBC were conducted within 600 min (1, 3, 5, 10,

15, 30, 60, 90, 120, 240, 360, and 600 min). The adsorption isotherm experiments were established with Cd^{2+} concentrations of 30–80 mg·L^{-1} (30, 40, 50, 60, 70, and 80 mg·L^{-1}) after a 4-h oscillation. After the oscillation, the mixture was filtered with the use of 0.45-μm filters.

The experimental design of the influence of various factors on the Cd(II) adsorption capacity of the MHBC was as follows: (i) ionic strength (the concentration of Na^+ was assessed at 0.01, 0.02, 0.03, 0.04, 0.05, and 0.06 mol·L^{-1}), (ii) dosage of adsorbent (0.01, 0.02, 0.03, 0.04, 0.05, and 0.06 g), (iii) concomitant ions (Cl^-, CO_3^{2-}, PO_4^{3-}, SO_4^{2-}, Mg^{2+}, Pb^{2+}, Cu^{2+}, and Zn^{2+}), and (iv) pH value (1, 2, 3, 4, 5, and 6).

The experiments aiming to evaluate the recycling capacity of the adsorbents were carried out by using 0.05 g MHBC, and 50 mL of the Cd^{2+} solution. The mixture was oscillated at 25°C and 200 rpm for 8 h, and then the adsorbents were separated by a filter. Subsequently, the adsorbents were dried in an oven at 70°C. Then, 0.05 g of the dried adsorbent was immersed in HNO_3 (0.1 mol·L^{-1}), and was used for desorption by oscillation under the same conditions. The above process was repeated five times.

For all adsorption experiments, three groups of parallel experiments were set.

2.4. Analysis methods and adsorption models

The concentration of Cd^{2+} was detected with flame atomic absorption spectrophotometer (novAA 350; Analytik Jena GmbH, Germany). The adsorption capacity and the removal percentage of Cd^{2+} by the adsorbent were calculated according to Eqs. (1) and (2):

$$q_t = \frac{\left(C_0 - C_t\right)V}{m} \tag{1}$$

$$\eta = \frac{C_0 - C_t}{C_0} \tag{2}$$

where q_t is the amount of Cd^{2+} adsorbed at the time of adsorption t (mg·g^{-1}), V is the volume of the solution (L), η is removal percentage is the removal percentage of Cd^{2+}, m is the mass of adsorbent (g), C_0 is the initial concentration of Cd^{2+} (mg·L^{-1}).

2.4.1. Adsorption kinetic model

Pseudo-first-order and pseudo-second-order models, as well as the Weber–Morris kinetic model were used to fit the adsorption experimental data. The specific equations were as follows, where the pseudo-first-order kinetic model equation was as Eq. (3), the pseudo-second-order kinetic model equation was as Eq. (4), and the Weber–Morris kinetic model equation was as Eq. (5):

$$q_t = q_e\left[1 - \exp\left(-k_1 t\right)\right] \tag{3}$$

$$\frac{t}{q_t} = \frac{1}{k_2 q_e^2} + \frac{t}{q_e} \tag{4}$$

$$q_t = k_{ip} t^{0.5} + C \tag{5}$$

where q_e is the equilibrium adsorption capacity (mg·g^{-1}), k_1 is the reaction constant of the pseudo-first-order kinetic model (min^{-1}), k_2 is the reaction constant of the pseudo-second-order kinetic model (g·mg^{-1}·min^{-1}), k_{ip} is the diffusion rate constant within the particle (mg·(g·min$^{0.5}$)$^{-1}$), and t is the adsorption time (min).

2.4.2. Isothermal adsorption model

The Langmuir model and the Freundlich model were used so as to fit and analyze the data. The equations were as follows, where the Langmuir model equation was as Eq. (6), the Freundlich model equation was as Eq. (7), and the Sips model equation was as Eq. (8):

$$\frac{C_e}{q_e} = \frac{1}{K_L q_m} + \frac{C_e}{q_m} \tag{6}$$

$$\ln q_e = \ln K_F + \frac{1}{n}\ln C_e \tag{7}$$

$$q_e = q_m \frac{K_S C_e^{1/n_s}}{1 + K_S C_e^{1/n_s}} \tag{8}$$

where q_e is the equilibrium adsorption capacity (mg·g^{-1}), q_m is the saturated adsorption capacity (mg·g^{-1}), C_e is the concentration of Cd^{2+} when the adsorption reaches equilibrium (mg·L^{-1}), K_L is the Langmuir adsorption coefficient, K_F is the Freundlich adsorption coefficient, and K_S is the Sips model coefficient, while n and n_s represent the nonlinear coefficients of the Langmuir and the Sips models (dimensionless), respectively [28].

3. Results and analysis

3.1. Adsorbent characterization

Fig. 1 presents the scanning electron microscopy results regarding the BC, the HBC, and the MHBC. BC (Fig. 1a and b) retained part of the eggshell calcium carbonate structure. Its particle size was obviously larger than that of HBC. Its surface was relatively flat, and there were some fine pores and cracks. HBC (Fig. 1c and d) had a rough surface with many small particles and bumps. This was characteristic of the successful loading of HAP. When compared to BC, MHBC (Fig. 1e and f) had a relatively rough surface, a clear texture, and an obviously porous structure. The EDS mapping (Fig. 1g) revealed that the main components of MHBC were C, O, and Ca, while the high proportion of Ca was due to the modification of calcium carbonate and HAP. The appearance of P and Mg resulted from the modification of the Mg-doped HAP.

The N_2 adsorption–desorption isotherms and the pore size distribution of BC and MHBC are listed in Fig. 2a and b. According to the IUPAC classification, the isotherms of BC and MHBC can be classified as type IV(a) isotherms

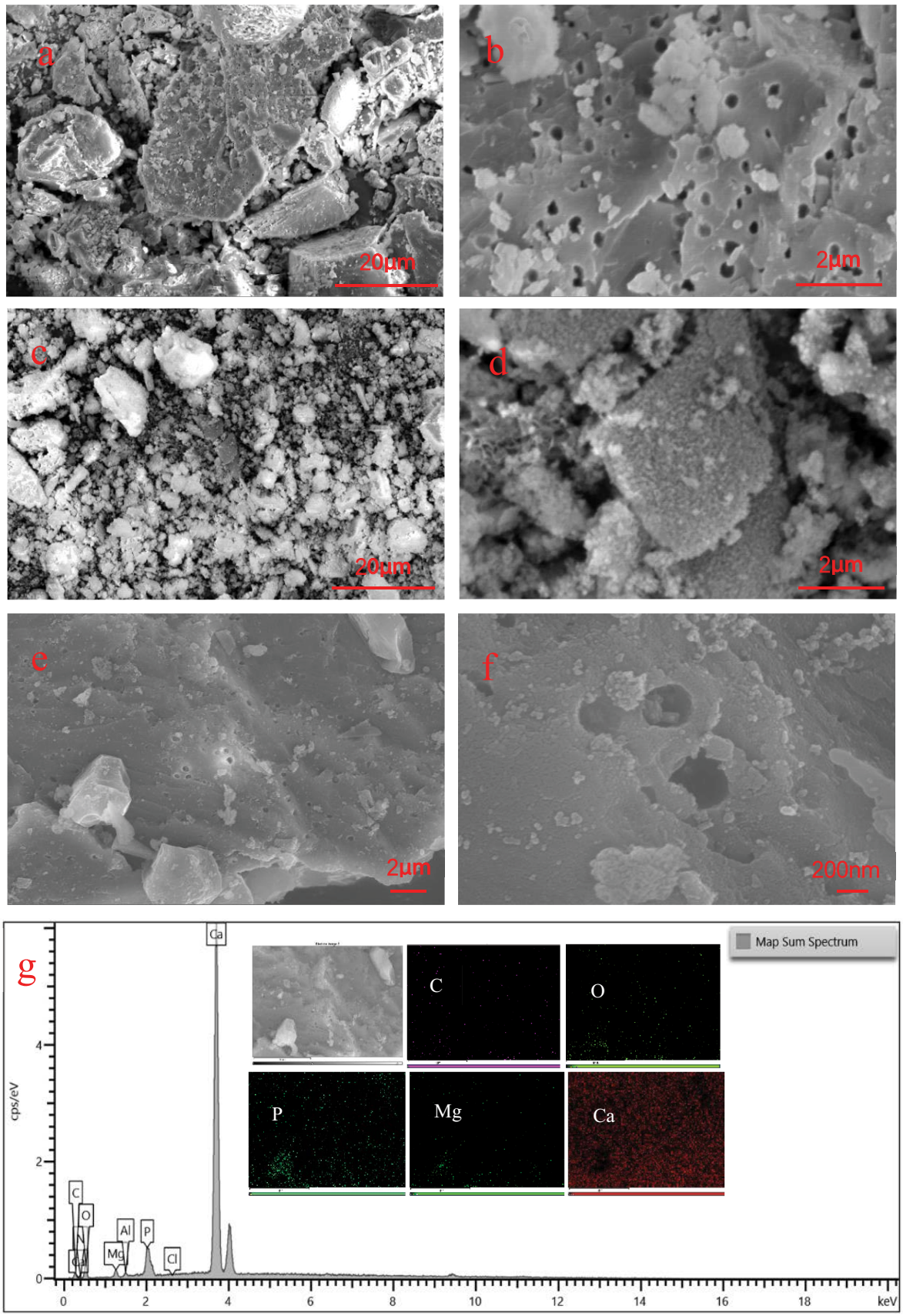

Fig. 1. SEM images of BC (a,b), HBC (c,d) and MHBC (e,f); EDS mapping of MHBC (g).

with type H_3 hysteresis loops, thereby indicating the existence of many mesopores [29]. However, the macropores that were not completely filled with pore condensate can also form the pore network. The pore size of the BC (Fig. 2a) was mainly in the range of 2.5–5 nm, while that of MHBC (Fig. 2b) was mainly in the range of 25–50 nm. This was consistent with their N_2 adsorption–desorption isotherms. As shown in Table 1, the specific surface area of MHBC was 3.0 times larger than that of BC, and the total pore volume was 4.9 times higher than that of BC, thereby leading to an increase in adsorption sites. The modification of HAP formed a cluster structure, and increased its specific surface area.

On the other hand, Mg^{2+} reduced the size of the microcrystals, and further increased the specific surface area [30]. The mechanism through which Mg^{2+} affects the HAP crystallization is that it is adsorbed on the surface of the formed ion clusters and the amorphous calcium phosphate primary particles (that prevent the further growth of these particles and the formation of a crystal structure), thereby reducing the size and the crystallinity of the microcrystals [31]. The dwarf bulges on the surface of MHBC can be explained by the traces left by Mg^{2+} while inhibiting crystallization. After modification, the pore structure of the MHBC changed greatly, and mesopores of about 36 nm were confirmed. At the same time, the small pore structure disappeared completely, thereby resulting into the indistinctive increase in the specific surface area and total pore volume of the MHBC.

Fig. 2c presents the FTIR spectra of BC, HBC, and MHBC before and after the adsorption of Cd^{2+}. The strong absorption peak at 1,425 and 711 cm^{-1} represents CO_3^{2-} [32], which resulted from the rich $CaCO_3$ in the eggshells. The characteristic peak at 3,458 cm^{-1} was the stretching vibration of the hydroxyl (–OH). The slight change of the peak height before and after the modification indicates the increase of the number of hydroxyl groups on the surface of HBC and MHBC. The new peak of HBC and MHBC at 1,043 cm^{-1} is the asymmetric elastic vibration absorption peak of PO_4^{3-} [33]. In addition, the absorption peaks at wavelengths 604 and 567 cm^{-1} were the tetrahedral symmetric

Table 1
Pore structure parameter of BC and MHBC.

Samples	Specific surface area (m^2/g)	Total pore volume (cm^3/g)	Most probable pore size (nm)
BC	2.866	0.0051	2.995
MHBC	8.665	0.0252	36.02

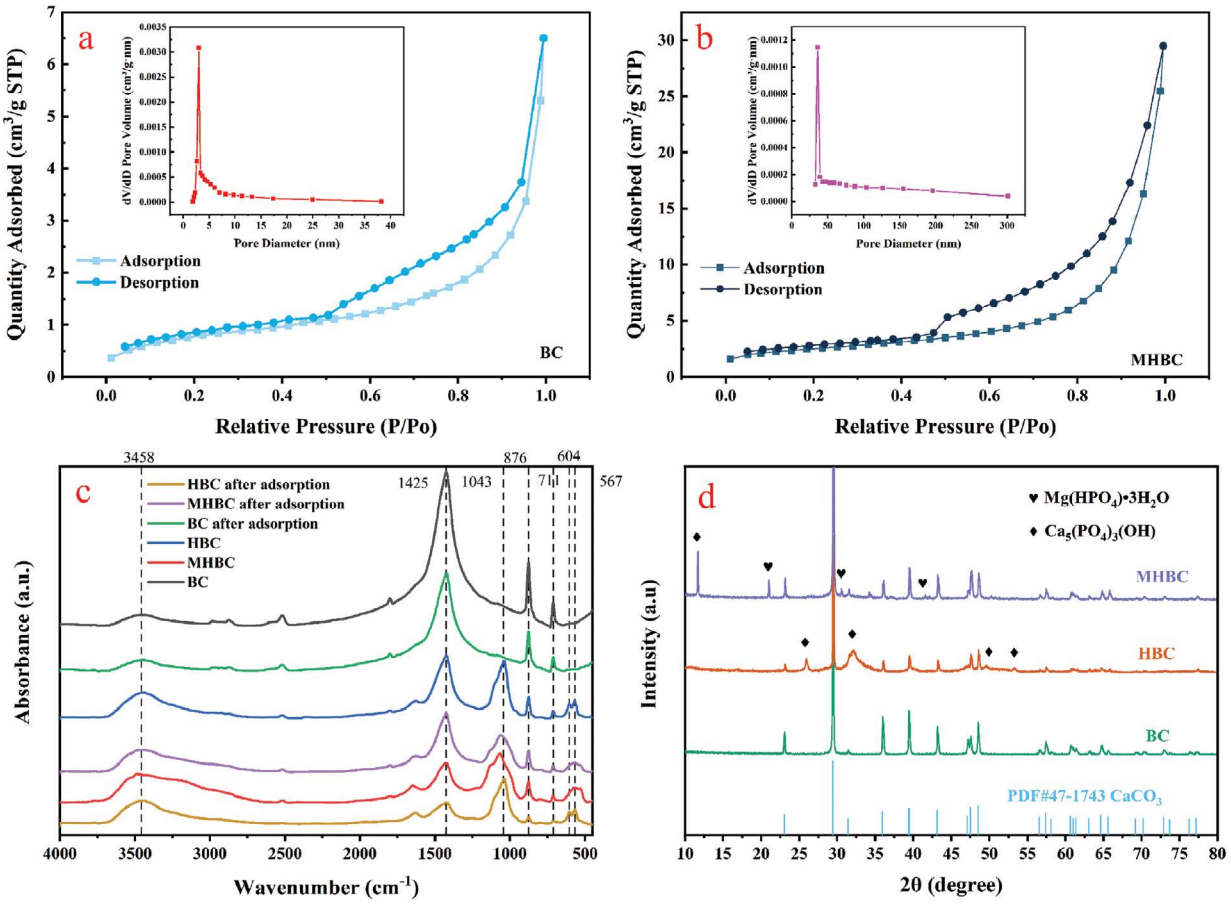

Fig. 2. The N_2 adsorption–desorption isotherms (a,b), the pore size distribution (a,b) of BC and MHBC, FTIR spectra of BC, HBC, and MHBC before and after absorption (c), XRD patterns of BC, HBC and MHBC (d).

stretching vibration peaks of PO_4^{3-} [34]. These functional groups reflect the structure of HAP. The sharp absorption peak at 876 cm^{-1} can be attributed to the swing of $=CH_2$.

The XRD patterns of BC, HBC and MHBC are presented in Fig. 2d. The diffraction peaks of BC at 2θ of 23.05°, 29.40°, 39.41°, and 43.16° are consistent with the crystal composition of $CaCO_3$ (PDF#47-1743). In contrast, the diffraction peaks of 2θ at 25.97°, 32.03°, 49.65°, and 53.26° correspond to the crystal plane of $Ca_5(PO_4)_3(OH)$ and were the characteristic peaks of HAP [35,36]. New diffraction peaks of 2θ at 21.02°, 30.57°, and 41.61° appearing on the MHBC pattern are the characteristic peaks of $Mg(HPO_4)\cdot 3H_2O$ [35]. These changes indicate that the HAP and the magnesium-doped HAP have successfully compounded with BC. Besides, the weakening of some characteristic peaks of the $CaCO_3$ of HBC and MHBC might be due to the destruction of its crystallization by the introduction of HAP, in a way that its diffraction peaks became unobvious.

3.2. Adsorption kinetics

As shown in Fig. 3a, the adsorption capacity of the three absorbents for Cd^{2+} increased with the passage of time. Moreover, the adsorption capacity of HBC and MHBC were much stronger than that of BC. The Cd^{2+} uptake by the HBC and MHBC was a two-step process, with an initial rapid phase at a contact time of 0–120 min, followed by a slower uptake phase until the equilibrium was reached. The modification of HAP greatly improved the adsorption rate of the adsorbent for Cd^{2+}, and shortened the time required for it to reach the adsorption equilibrium. The equilibrium adsorption capacities of BC, HBC, and MHBC were about 4.82, 35.82, and 49.41 $mg\cdot g^{-1}$, respectively. The equilibrium adsorption capacity of MHBC was 1.357 times higher than that of HBC, thereby illustrating that the adsorption capacity of MHBC was also improved after the addition of Mg^{2+}. According to the results of SET and BET analysis, it was speculated that the increase in the specific surface area and the adsorption site was one of the reasons leading to the improvement of the adsorption capacity of HBC and of MHBC. Additionally, the loading of Mg^{2+} and the increase of oxygen-containing functional groups might also enhance the adsorption capacity of MHBC and HBC. At the initial stage of adsorption, the adsorption amount increased rapidly because the adsorption mainly occurred on the outer surface of adsorbent. As the reaction time increased, the active site was occupied, and Cd^{2+} gradually diffused into the pore structure such as the slit, and further reacted with the internal active site. Finally, the adsorption process reached equilibrium [37].

Pseudo-first-order and pseudo-second-order models were used in order to fit the experimental data (Fig. 3a), and the relevant fitting parameters are shown in Table 2. According to the presented data, the values of R^2 for the pseudo-second-order kinetic model developed for the herein assessed three metal-sorbent systems, were relatively high in comparison to value of R^2 for the pseudo-first-order model; a finding suggesting that the pseudo-second-order model was the most suitable model for all adsorption systems. In addition, the equilibrium sorption capacities

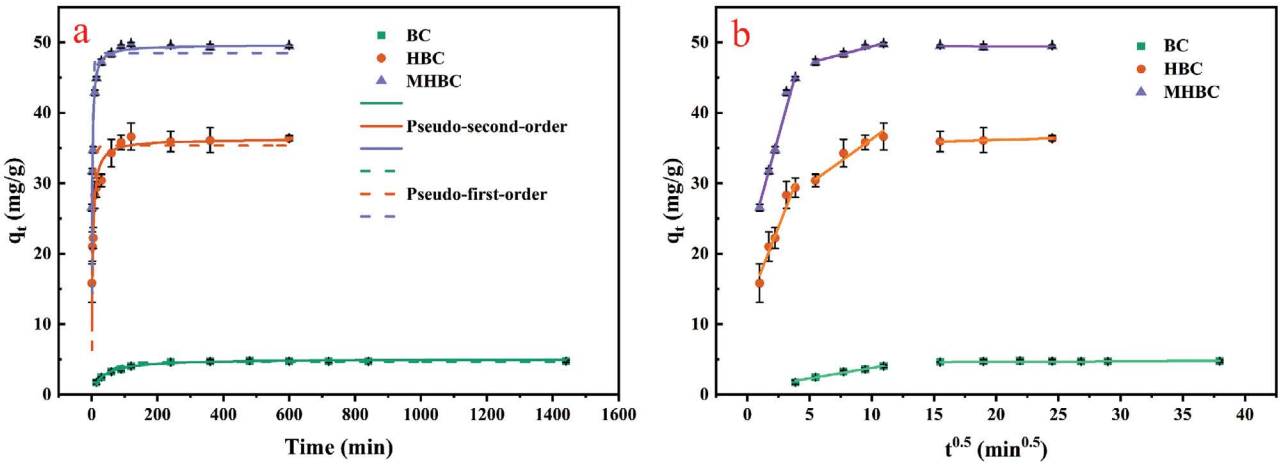

Fig. 3. Adsorption kinetics for Cd^{2+} by BC, HBC, and MHBC (a) (pseudo-first-order model and pseudo-second-order model fitting) (pH 6, 25°C); Fitting curves of Weber–Morris model (b).

Table 2
Parameters of adsorption kinetics

Adsorbent	Pseudo-first-order equation			Pseudo-second-order equation		
	q_e ($mg\cdot g^{-1}$)	k_1 (min^{-1})	R_1^2	q_e ($mg\cdot g^{-1}$)	k_2 ($g\cdot mg^{-1}\cdot min^{-1}$)	R_2^2
BC	4.66	0.0211	0.946	4.96	0.0067	0.986
HBC	33.97	0.2865	0.726	35.49	0.0133	0.910
MHBC	47.49	0.4169	0.693	49.13	0.0156	0.916

of BC, HBC, and MHBC calculated by the pseudo-second-order kinetic equation fitted well to the experimental values, and the q_e values of the pseudo-first-order equation were significantly lower for all adsorbents [38]. Our data revealed that the adsorption of Cd^{2+} in solution might be mainly affected by chemisorption, thereby suggesting that the major interactions between the adsorbent and the Cd^{2+} could be through chemical complexation [39,40].

In order to further determine the mechanism of the Cd^{2+} adsorption on the material, the Weber–Morris kinetic model was used in order to fit the experimental results (Fig. 3b and Table 3). The adsorption process of Cd^{2+} on HBC and MHBC was divided into three steps; namely, the film diffusion, the intraparticle diffusion, and the adsorption equilibrium over time. The adsorption process of BC was divided into two obvious steps: the film diffusion and the adsorption equilibrium. Film diffusion occurred on the surface of the adsorbent, and at that stage, the slope of the straight line was larger, and the adsorption rate was faster. A comparison of the kinetic parameters and characteristics of the porous structure allowed us to conclude that the higher values of the diffusion rate constant (k_{ip}) at the film diffusion stage and the initial velocity of the sorption for HBC and MHBC, may be due to their larger specific surface area [38]. In the intraparticle diffusion step, the adsorption on the surface of the adsorbent was basically completed, and Cd^{2+} began to diffuse to the inner surface of the adsorbent and to further react with it. The *C* value at this stage was higher than that of the first step, thereby reflecting the increase of the boundary layer resistance and the gradual decrease of the adsorption rate, which meant that the intraparticle diffusion was the main speed limiting step of the adsorption by the modified adsorbent [41]. At the end of the intraparticle diffusion, the adsorption tended to be saturated. In addition, the slow film diffusion rate (lower slope) and the lack of the intraparticle diffusion step were the main reasons for the low adsorption capacity of BC, that could be attributed to its low surface area and total pore volume. In the first and the second-stages of HBC and MHBC, the fitting curves did not pass through the origin, thereby indicating that the intraparticle diffusion was not the only rate control factor [37,42].

3.3. Effect of the adsorption environment

With the increase of the initial concentration, the adsorption capacity increased rapidly at first, and then the increase was gradually reduced (Fig. 4a). When the initial concentration changed from 70 to 80 $mg·L^{-1}$, the growth of adsorption capacity was 2.85 $mg·g^{-1}$; only 27% of that of the previous period (30–40 $mg·L^{-1}$). It could be considered that the adsorption sites of Cd^{2+} on MHBC were certain. When the initial concentration was low, only a part of the adsorption sites was occupied by Cd^{2+}. With the increase of the initial concentration, the number of Cd^{2+} increased, and the adsorption sites occupied by Cd^{2+} also increased gradually, so that the removal capacity increased gradually. The number of adsorption sites occupied by Cd^{2+} was closer to the maximum number of adsorption sites of the adsorbent, while the growth of the removal capacity was smaller and, finally, tended to be stable. Therefore, when the initial concentration was low, the removal rate of Cd^{2+} was relatively high. When the Cd^{2+} in the aqueous reached a certain concentration, the adsorption site became saturated. In this state, the MHBC could not continue to adsorb Cd^{2+}, and the removal percentage would decrease, as shown in Fig. 4a.

It can be seen from Fig. 4b that with the growth of dosage, the adsorption capacity gradually decreased, and the removal percentage continued to rise from 50% to 98.43%. With the increase of the dosage, the unused spare active sites on MHBC increased, while the aggregation and the overlap of these active sites led to a reduction of the adsorption surface area [43]. Moreover, the increase of the adsorption capacity couldn't catch up with the growth of the adsorbent dosage, thereby resulting in a decrease of the Cd^{2+} unit adsorption capacity of the MHBC in water. This meant that MHBC was an adsorbent that could achieve a high adsorption effect with a low dose. Considering the removal efficiency and the economic benefit, the optimal dosage in this study was set at 1.0 $g·L^{-1}$. Of course, further consideration is required when dealing with the actual wastewater treatment process.

The Cd^{2+}-removal percentage and the removal capacity of the MHBC decreased with the increase of the Na^+ concentration (Fig. 4c). This could be attributed to the ion exchange between Na^+ in solution and the Cd^{2+} adsorbed on MHBC, or could be due to the sodium ions exerting a compression upon the thickness of the double electric layer, thereby weakening the electrostatic interaction between MHBC and Cd^{2+} in the solution [44]. In addition, it is known that the dense hydration shell formed on the surface of MHBC after Na^+ adsorption can prevent the adsorption of Cd^{2+} on the surface of MHBC [45].

The effect of the pH value on the adsorption of Cd^{2+} by MHBC is shown in Fig. 4d. The changes of the removal

Table 3
Fitting parameters of Weber–Morris model

Step	Parameter	BC	HBC	MHBC
Step 1	k_{ip} ($mg·(g·min^{0.5})^{-1}$)	0.3129	4.8135	6.6838
	C ($mg·g^{-1}$)	0.6558	11.7923	20.0963
	R^2	0.981	0.954	0.978
Step 2	k_{ip} ($mg·(g·min^{0.5})^{-1}$)	Adsorption equilibrium	1.1423	0.4817
	C ($mg·g^{-1}$)		24.6595	44.5929
	R^2		0.918	0.965
Step 3	N/A	N/A	Adsorption equilibrium	Adsorption equilibrium

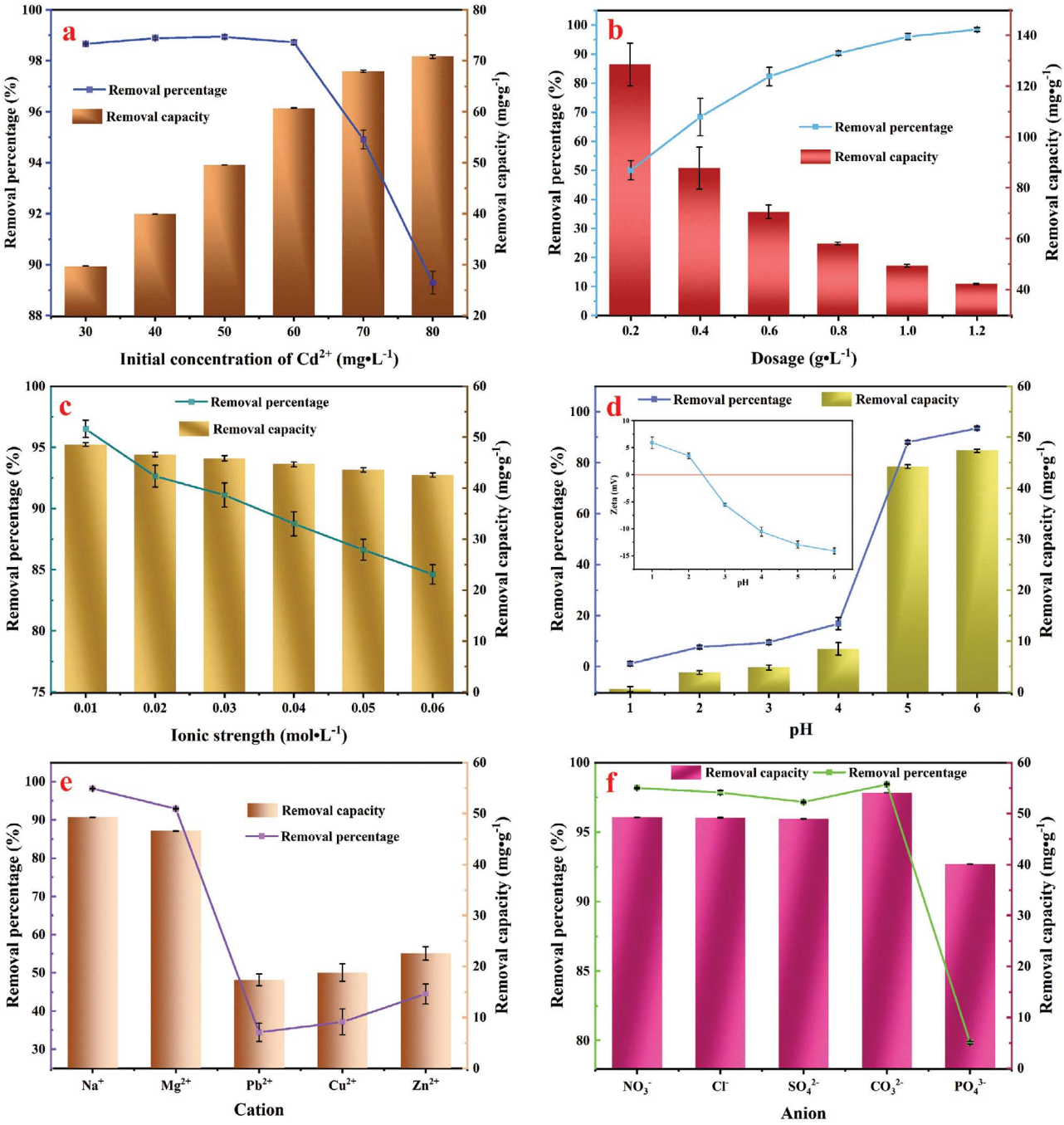

Fig. 4. Influence of initial concentration, dosage, ionic strength, pH, cation and anion on Cd^{2+} adsorption by MHBC.

percentage and the removal capacity were consistent. The range of pH 4–5 was an obvious dividing line. When the pH was ≤4, the adsorption capacity was very small, and the removal percentage was very low. When the pH was ≥5, both the adsorption capacity and the removal percentage increased rapidly. Under low pH conditions, a large number of H^+ in the solution could occupy part of the adsorption sites and compete with Cd^{2+} [46]. On the other hand, both the H^+ and the Cd^{2+} adsorbed on the surface of MHBC might generate an electrostatic repulsion with Cd^{2+} in the solution, thereby reducing the removal capacity of Cd^{2+} on MHBC. However, with the increase of pH and the decrease of H^+, the adsorption sites on the MHBC bound to Cd^{2+} in solution, thereby increasing the removal capacity of Cd^{2+}. The change of the MHBC surface potential has greatly improved its adsorption capacity; an observation indicating that the electrostatic action was likely to be one of the adsorption mechanisms. However, when combined with the potential diagram embedded in Fig. 4d, the electrostatic action cannot fully explain the smiling change in the adsorption capacity

when the pH across the zero potential point changed from 2 to 3, or the huge change of the adsorption capacity when the pH changed from 4 to 5. This might involve an exchange between cations on the MHBC surface and cations in the solution during the adsorption process.

The influence of concomitant ions on the adsorption of Cd^{2+} by MHBC is shown in Fig. 4e and f. When compared with anions, cations had a greater effect on the adsorption effect. The anion CO_3^{2-} slightly enhanced the removal capacity, possibly because Na_2CO_3 provided CO_3^{2-}, that was conducive to the formation of insoluble $CdCO_3$ [47]. When PO_4^{3-} existed at a certain concentration, the removal capacity decreased to a certain extent, which could be due to the interference between PO_4^{3-} in the solution and PO_4^{3-} on the surface of MHBC. The inhibitory effect of metal cations on the adsorption of Cd^{2+} by MHBC was mainly due to the competitive adsorption occurring between metal cations, especially between heavy metal ions [48]. When combined with the experimental findings on the effect of the ionic strength on adsorption, it could be inferred that other metal cations adsorbed on the surface of MHBC would repel Cd^{2+}. The existence of Pb^{2+}, Cu^{2+}, and Zn^{2+} reduced the removal capacity of MHBC for Cd^{2+} from 49.23 to 22.54 $mg \cdot g^{-1}$. In contrast, Mg^{2+} had little effect on its adsorption capacity. This was because Mg^{2+} exhibited a stronger covalent nature compared to Pb^{2+}, Cu^{2+} and Zn^{2+}, hence the Mg^{2+} displayed a stronger hydration that reduced their interaction with the surface of MHBC [48,49].

3.4. Adsorption isotherms

The adsorption capacity of the three adsorbents for Cd^{2+} increased with the increase of the Cd^{2+} equilibrium concentration in the solution, and this trend was gradually abated (Fig. 5a). This feature was obvious in the isotherms of HBC and MHBC; especially in the isotherm of MHBC during the early stage, when it was nearly vertical. However, the increase of the adsorption capacity of BC was smaller, which indicated that the adsorption capacity of the MHBC for Cd^{2+} was much stronger than that of BC. The Langmuir, Freundlich, and Sips isothermal models were used so as to fit the isothermal adsorption data (Fig. 5b–d). The fitting parameters of the three models are provided in Table 4. Fig. 5 and Table 4 show that the three models had good fitting effects on the isothermal adsorption of BC ($R^2 > 0.967$). However, for HBC and MHBC, the Sips model was able to

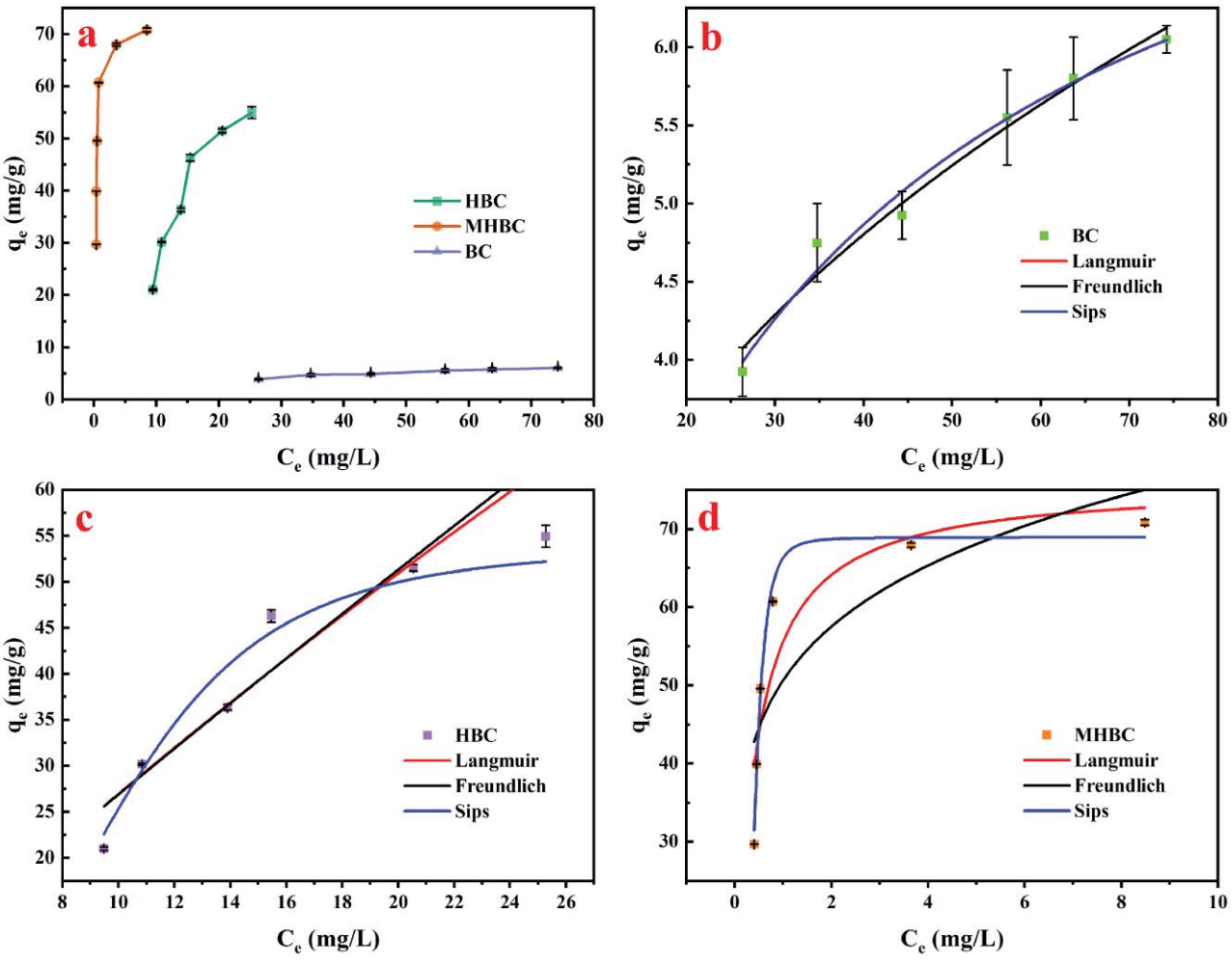

Fig. 5. Isothermal curves (a) and fitting curves of Langmuir, Freundlich and Sips isothermal models (b–d) (pH 6, 25°C).

better fit their isothermal adsorption data (when compared to the Langmuir and the Freundlich models). The Sips model is an empirical model obtained by integrating the Langmuir model and the Freundlich model, and has the characteristics of both models. In fact, it has a strong applicability to various adsorption systems with different adsorbent concentrations and surface properties [50,51]. The maximum adsorption capacity of BC, HBC, and MHBC calculated from the Sips model were 8.414, 58.811, and 68.898 mg·g^{-1}, respectively. This illustrates that there might be a combination of monolayer and multilayer adsorption involved in the adsorption of Cd^{2+} in solution by HBC and MHBC. In other words, in addition to a complex cooperation, HBC and MHBC might also be able to remove Cd^{2+} in solution through electrostatic interaction and physical adsorption.

In an attempt to further evaluate the ability of MHBC to remove Cd^{2+}, the comparison data for typical calcium–magnesium phosphates with and without apatite structures were presented (Table 5). Although the adsorption capacity of MHBC was not as good as that of the phosphate-modified dolomite material, the eggshell as a raw material is easier to collect, transport, and process (grinding, calcination, etc.) than the natural dolomite, which is an advantage. Moreover, the modification significantly improved the adsorption capacity of the eggshell, so that it can efficiently remove Cd^{2+} from water, thereby suggesting that the MHBC is a material with a certain development potential in the field of urban industrial wastewater treatment.

3.5. Reuse performance

In order to evaluate the sustainability of the MHBC's removal capacity for Cd^{2+}, three cyclic adsorption experiments were performed. As shown in Fig. 6, the removal capacity (q_e) and the removal percentage of Cd^{2+} by MHBC declined uniformly with the increase in the number of cycles. However, after three cycles, the removal percentage of Cd^{2+} by MHBC still reached 78.75%. Initially, the amount of Cd^{2+} adsorbed per gram of the MHBC was 49.44 (±0.19) mg·g^{-1}, and it was reduced to 39.44 (±0.59) mg·g^{-1} after the third adsorption–desorption cycle.

The adsorption capacity of the Cd^{2+} decreased by 20.2% after the third cycle, under the given desorption conditions. That might be due to the loss in desorption and cleaning process of the materials. At the same time, the change of the physical and chemical properties of the adsorbents, including the reduction of their specific surface area and the weakening of their surface functional groups caused by a change of the pore structure, cannot be excluded. However, insignificant changes in the FTIR spectra before and after the MHBC adsorption indicate that the interaction between the MHBC and Cd^{2+} is weak, thereby suggesting that an effective desorption of Cd^{2+} is possible. Therefore, if the desorption conditions (such as the use of ultrasound or desorption agents) are improved, the adsorbed Cd^{2+} is expected to be successfully removed from the surface. Thus, most of the adsorption sites can easily be adsorbed again. This effort should be taken into account by future studies.

Table 4
Fitting parameters of isothermal adsorption models

Isotherm models	Parameters	BC	HBC	MHBC
Langmuir	q_m (mg·g^{-1})	8.444	189.256	75.844
	K_L (L·mg^{-1})	0.0340	0.0174	2.733
	R^2	0.976	0.881	0.800
Freundlich	K_F (L·mg^{-1})	1.1257	4.5236	50.6178
	n	2.542	1.262	5.435
	R^2	0.967	0.863	0.632
Sips	q_m (mg·g^{-1})	8.414	58.811	68.898
	K_S (L·g^{-1})	0.0336	0.0004	25.2891
	n_s	0.994	0.308	0.268
	R^2	0.968	0.958	0.981

3.6. Adsorption mechanism

When combined with the characterization and the adsorption experimental results, the key factors determining the removal efficiency of Cd^{2+} by MHBC were the pH value of the solution and the active groups identified on the surface of the adsorbent. The characterization revealed that the surface morphology of the MHBC changed little after the modification, and the specific surface area and pore volume of the MHBC were not large. Pore-filling might be the adsorption mechanism of BC with regard to Cd^{2+}, but it was not the main adsorption mechanism of MHBC. Based

Table 5
Sorption capacity of different materials towards Cd^{2+}

Adsorbent	Sorption capacity (mg·g^{-1})	References
Modified phosphate dolomite	1218.5	[52]
Ca-Mg phosphate based on dolomite	241.7	[53]
MHBC	49.4	This work

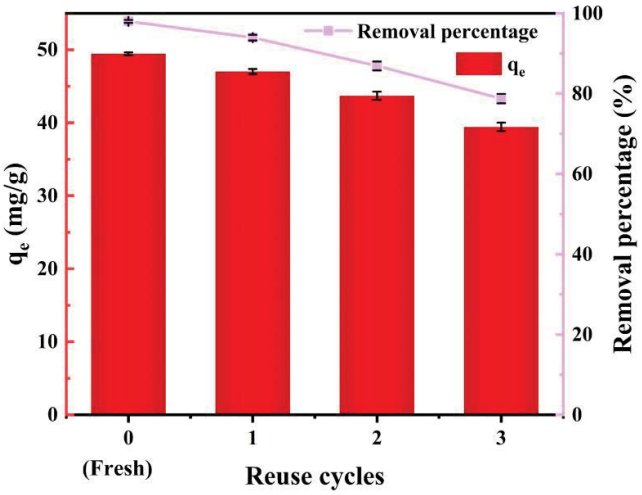

Fig. 6. Cyclic adsorption performance of MHBC (pH 6, 25°C).

on the results of the material characterization and the batch adsorption experiments, it could be suggested that the adsorption of Cd^{2+} by MHBC was mainly due to chemical adsorption, supplemented by physical adsorption (Fig. 7). Surface complexation, ion exchange, and dissolved precipitation have been suggested to be important mechanisms for the removal of metal ions from HAP materials [54]. In this study, if the dissolved precipitation plays a major role, the increase of H^+ in the solution with a low pH value should have promoted the occurrence of dissolution and, thus, should have promoted the removal of Cd^{2+}; however, the facts support the opposite. Thus, surface complexation and ion exchange should be considered further.

The –OH group have lone pair electrons, and the vacant orbital existing in Cd^{2+} can accept the lone pair electrons of –OH, and can form coordination complexes [55,56]. Fig. 2e shows that the peak area at 3,450–3,500 cm^{-1} decreased after the MHBC absorbs Cd^{2+}, which is the stretching vibration peak of the O–H bond, thereby indicating that the amount of –OH was reduced and proving that the –OH groups have reacted with Cd^{2+}. The complexation reaction can be expressed as follows:

$$2\text{MHBC-OH} + \text{Cd}^{2+}(\text{aq}) \rightarrow (\text{MHBC-O})_2 - \text{Cd} + 2\text{H}^+(\text{aq}) \quad (9)$$

The change of the adsorption capacity with pH can also be explained by Eq. (9), in addition to the electrostatic action. When the pH was low and the number of H^+ in the solution was high, the reaction would move toward the direction of Cd^{2+} formation. Otherwise, it would promote the adsorption of Cd^{2+} by MHBC.

For the cation-doped HAP, the closer the ionic radius was to the radius of Ca^{2+}, the higher the relative doping rate would be [45]. The radii of the calcium ion, the magnesium ion, and the cadmium ion were 0.099, 0.072, and 0.097 nm, respectively. Due to the difference between the radii of Mg^{2+} and Ca^{2+}, the crystallization of MHBC would be affected to a greater extent, thereby making it unstable. On the one hand, the Mg^{2+} substitution inhibited the formation of crystalline HAP, and might lead to the formation of low-crystalline material or completely prevent the phase transformation to HAP [31,57], thereby increasing the specific surface area. On the other hand, when Cd^{2+} with similar ionic radius to Ca^{2+} appeared, they were more likely to combine and generate stable structures (similar to HAP) on the surface of the adsorbent. Therefore, Cd^{2+} could swap with Mg^{2+} in the Mg-doped HAP structure on the surface of MHBC [27]. The fact that Mg^{2+} had the smallest influence on the adsorption of Cd^{2+} by MHBC, also proves the possibility of an ion exchange. The reaction can be expressed as follows:

$$5\text{Ca}^{2+} + 6\text{NH}_4^+ + 3\text{HPO}_4^{2-} + 4\text{NH}_3 \cdot \text{H}_2\text{O} \rightarrow \text{Ca}_5(\text{PO}_4)_3\text{OH}\downarrow + 10\text{NH}_4^+ + 3\text{H}_2\text{O} \quad (10)$$

$$5\text{Mg}^{2+} + 6\text{NH}_4^+ + 3\text{HPO}_4^{2-} + 4\text{NH}_3 \cdot \text{H}_2\text{O} \rightarrow \text{Mg}_5(\text{PO}_4)_3\text{OH}\downarrow + 10\text{NH}_4^+ + 3\text{H}_2\text{O} \quad (11)$$

$$x\text{Cd}^{2+} + \text{Mg}_{10}(\text{PO}_4)_6(\text{OH})_2 \rightarrow \text{Cd}_x\text{Mg}_{(10-x)}(\text{PO}_4)_6(\text{OH})_2 + x\text{Mg}^{2+} \quad (12)$$

4. Conclusion

By using eggshell as a raw material, a modified adsorbent (MHBC) was successfully prepared by substituting part of the calcium in the HAP with magnesium, and by

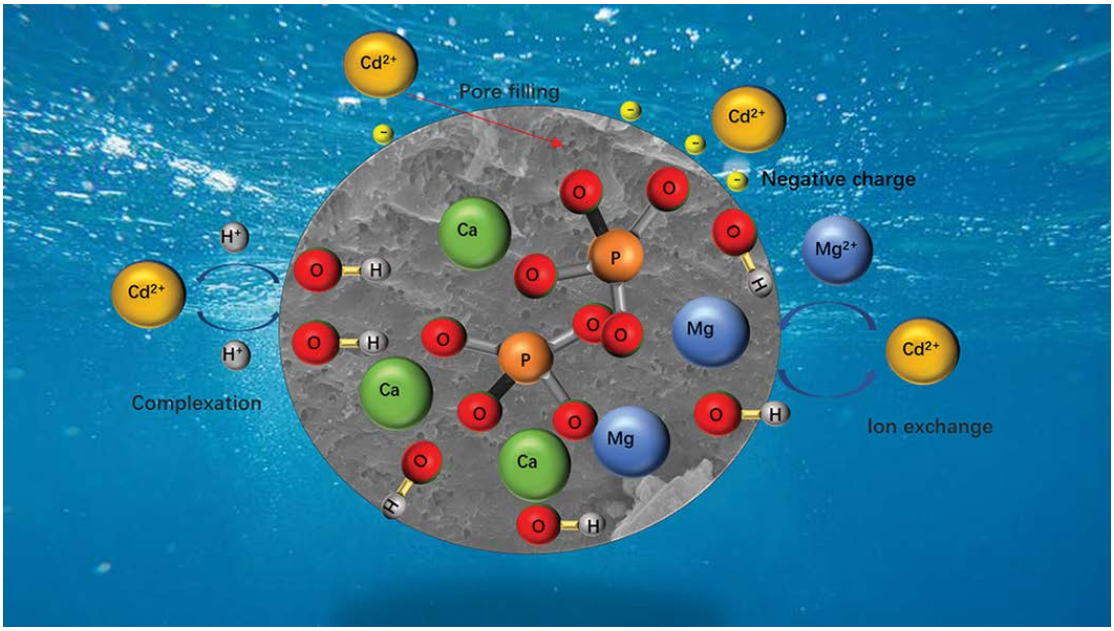

Fig. 7. Schematic diagram of adsorption mechanism of MHBC on Cd^{2+} in water.

combining it with the original adsorbent (BC). MHBC was able to quickly adsorb the Cd^{2+} in water, and to reach an adsorption equilibrium in 60 min. Its equilibrium adsorption capacity was 49.70 $mg \cdot g^{-1}$, which is 10 times that of BC. The particle size, surface area, and total pore volume of MHBC were found increased. The adsorption of Cd^{2+} by MHBC was more consistent with the pseudo-second-order kinetic model and the Sips isothermal model. The adsorption process was mainly controlled by a chemical mechanism, and monolayer and multilayer adsorption co-existed at the same time. The major interactions involved between MHBC and Cd^{2+} could be chemical complexation, ion exchange, and electrostatic attractions. The removal capacity of MHBC for Cd^{2+} rose and declined with the increase of the initial concentration and dosage, respectively. With the increase of the value of pH from 1 to 6, the removal percentage of Cd^{2+} increased greatly. The competitive adsorption of Mg^{2+}, Pb^{2+}, Cu^{2+}, and Zn^{2+} were able to inhibit the adsorption of Cd^{2+} by MHBC. The repeated adsorption–desorption test revealed that the MHBC could still efficiently adsorb Cd^{2+} after desorption, and its reuse was good. These results indicate that MHBC can effectively remove Cd^{2+} from a solution. They also offer a novel approach to the disposal and utilization of waste eggshells. Based on our findings, we believe that: (i) the adsorption capacity of the MHBC can be further improved by modification, (ii) its effect on metal ions other than Cd^{2+} should be explored, and (iii) suitable desorption methods are required in order to restore the adsorption capacity of the MHBC.

CRediT authorship contribution statement

Xiangyi Gong: Development or design of methodology, Writing – review & editing, Methodology, Funding acquisition. Dekang Meng: Data curation, Writing – original draft, Investigation, Formal analysis, Methodology, Writing – review & editing. Zhang Peng: Methodology, Data curation, Investigation. Zeya Wang: Conceptualization, Visualization, Project administration. Dajun Ren: Validation, Writing – review and editing. Fengying Wu: Investigation, Data curation.

Disclosure statement

No potential conflict of interest was reported by the author(s).

Acknowledgments

This research was financially supported by the Open Research Program of Hubei Key Laboratory for Efficient Utilization and Agglomeration of Metallurgic Mineral Resources, Wuhan University of Science and Technology (Grant No. 2020zy003), the Open Research Fund of Hubei Key Laboratory of Mine Environmental Pollution Control & Remediation, Hubei Polytechnic University (No. 2018104), and the Wuhan Science and Technology Planning Project (Grant No. 2020020601012274).

References

[1] X. Wang, W. Cui, M. Wang, Y. Liang, G. Zhu, T. Jin, X. Chen, The association between life-time dietary cadmium intake from rice and chronic kidney disease, Ecotoxicol. Environ. Saf., 211 (2021) 111933, doi: 10.1016/j.ecoenv.2021.111933.
[2] I. Suhani, S. Sahab, V. Srivastava, R.P. Singh, Impact of cadmium pollution on food safety and human health, Curr. Opin. Toxicol., 27 (2021) 1–7, doi: 10.1016/j.cotox.2021.04.004.
[3] D.L. Knoell, T.A. Wyatt, The adverse impact of cadmium on immune function and lung host defense, Semin. Cell Dev. Biol., 115 (2020) 70–76.
[4] M. Mahmood, M.M. Barbooti, A. Balasim, A. Altameemi, M.N. Al-Terehi, N. Al-Shuwaiki, Removal of heavy metals using chemicals precipitation, Eng. Technol. J., 29 (2011) 595–612.
[5] R. Kumar, J. Chawla, Removal of cadmium ion from water/wastewater by nano-metal oxides: a review, Water Qual. Exposure Health, 5 (2014) 215–226.
[6] R. Leyma, S. Platzer, F. Jirsa, W. Kandioller, R. Krachler, B.K. Keppler, Novel thiosalicylate-based ionic liquids for heavy metal extractions, J. Hazard. Mater., 314 (2016) 164–171.
[7] A. Almasian, M. Giahi, G.C. Fard, S.A. Dehdast, L. Maleknia, Removal of heavy metal ions by modified PAN/PANI-nylon core-shell nanofibers membrane: filtration performance, antifouling and regeneration behavior, Chem. Eng. J., 351 (2018) 1166–1178.
[8] B. Bansod, T. Kumar, R. Thakur, S. Rana, I. Singh, A review on various electrochemical techniques for heavy metal ions detection with different sensing platforms, Biosens. Bioelectron., 94 (2017) 443–455.
[9] M.A. Barakat, New trends in removing heavy metals from industrial wastewater, Arabian J. Chem., 4 (2011) 361–377.
[10] M. Owlad, M.K. Aroua, W.M.A.W. Daud, Hexavalent chromium adsorption on impregnated palm shell activated carbon with polyethyleneimine, Bioresour. Technol., 101 (2010) 5098–5103.
[11] C. Gutiérrez, H.K. Hansen, P. Hernández, C. Pinilla, Biosorption of cadmium with brown macroalgae, Chemosphere, 138 (2015) 164–169.
[12] Y. Chen, H. Wang, W. Zhao, S. Huang, Four different kinds of peels as adsorbents for the removal of Cd(II) from aqueous solution: kinetics, isotherm and mechanism, J. Taiwan Inst. Chem. Eng., 88 (2018) 146–151.
[13] B.B. Palabıyık, H. Selcuk, Y.A. Oktem, Cadmium removal using potato peels as adsorbent: kinetic studies, Desal. Water Treat., 172 (2019) 148–157.
[14] S. Afroze, T.K. Sen, A review on heavy metal ions and dye adsorption from water by agricultural solid waste adsorbents, Water Air Soil Pollut., 229 (2018) 225, doi: 10.1007/s11270-018-3869-z.
[15] D. Purkayastha, U. Mishra, S. Biswas, A comprehensive review on Cd(II) removal from aqueous solution, J. Water Process Eng., 2 (2014) 105–128.
[16] K. Pyrzynska, Removal of cadmium from wastewaters with low-cost adsorbents, J. Environ. Chem. Eng., 7 (2019) 102795, doi: 10.1016/j.jece.2018.11.040.
[17] P. Sudhakar, I.D. Mall, V.C. Srivastava, Adsorptive removal of bisphenol-A by rice husk ash and granular activated carbon—a comparative study, Desal. Water Treat., 57 (2016) 12375–12384.
[18] V. Vandeginste, Food waste eggshell valorization through development of new composites: a review, Sustainable Mater. Technol., 29 (2021) e00317, doi: 10.1016/j.susmat.2021.e00317.
[19] Y. Feng, B. Ashok, K. Madhukar, J.M. Zhang, J. Zhang, K. Obi Reddy, A. Varada Rajulu, Preparation and characterization of polypropylene carbonate bio-filler (eggshell powder) composite films, Int. J. Polym. Anal. Charact., 19 (2014) 637–647.
[20] P.S. Katha, Z. Ahmed, R. Alam, B. Saha, A. Acharjee, M. Safiur Rahman, Efficiency analysis of eggshell and tea waste as low cost adsorbents for Cr removal from wastewater sample, S. Afr. J. Chem. Eng., 37 (2021) 186–195.
[21] S.M. Prabhu, S.S. Elanchezhiyan, G. Lee, A. Khan, S. Meenakshi, Assembly of nano-sized hydroxyapatite onto graphene oxide sheets via in-situ fabrication method and its prospective application for defluoridation studies, Chem. Eng. J., 300 (2016) 334–342, 1385–8947.
[22] B. Gayathri, N. Muthukumarasamy, D. Velauthapillai, S.B. Santhosh, V. Asokan, Magnesium incorporated hydroxyapatite nanoparticles: preparation, characterization,

antibacterial and larvicidal activity, Arabian J. Chem., 11 (2018) 645–654.
[23] P. Madhavasarma, P. Veeraragavan, S. Kumaravel, M. Sridevi, Studies on physiochemical modifications on biologically important hydroxyapatite materials and their characterization for medical applications, Biophys. Chem., 267 (2020) 106474, doi: 10.1016/j.bpc.2020.106474.
[24] L. Chen, K.-S. Zhang, J.-Y. He, W.-H. Xu, X.-J. Huang, J.-H. Liu, Enhanced fluoride removal from water by sulfate-doped hydroxyapatite hierarchical hollow microspheres, Chem. Eng. J., 285 (2016) 616–624.
[25] A. Oulguidoum, H. Bouyarmane, A. Laghzizil, J.-M. Nunzi, A. Saoiabi, Development of sulfonate-functionalized hydroxyapatite nanoparticles for cadmium removal from aqueous solutions, Colloid Interface Sci. Commun., 30 (2019) 100178, doi: 10.1016/j.colcom.2019.100178.
[26] C.-H. Ooi, Y.P. Ling, S.-Y. Pung, F.-Y. Yeoh, Mesoporous hydroxyapatite derived from surfactant-templating system for *p*-Cresol adsorption: physicochemical properties, formation process and adsorption performance, Powder Technol., 342 (2019) 725–734.
[27] H. Li, Q. Jiang, S. Jiang, J. Qu, Z. Jiang, Y. Zhang, Study on the adsorption performance of Fe(II)-doped hydroxyapatite for Pb(II) in aqueous solution, J. Agric. Resour. Environ., (2021) 1–15, doi: 10.13254/j.jare.2021.0211.
[28] H. He, Z. Zhu, J. Liu, Y. Zhu, Q. Yan, Y. Liu, N. Mo, H. Xuan, W. Wei, Removal of Pb^{2+} from aqueous solution by magnesium–calcium hydroxyapatite adsorbent, Environ. Sci., 40 (2019) 4081–4090.
[29] M. Thommes, K. Kaneko, A.V. Neimark, J.P. Olivier, F. Rodriguez-Reinoso, J. Rouquerol, K. Sing, Physisorption of gases, with special reference to the evaluation of surface area and pore size distribution (IUPAC Technical Report), Pure Appl. Chem., 87 (2015) 1051–1069.
[30] A.I. Ivanets, N.V. Kitikova, I.L. Shashkova, M. Yu. Roshchina, V. Srivastava, M. Sillanpää, Adsorption performance of hydroxyapatite with different crystalline and porous structure towards metal ions in multicomponent solution, J. Water Process Eng., 32 (2019) 100963, doi: 10.1016/j.jwpe.2019.100963.
[31] H. Ding, H. Pan, X. Xu, R. Tang, Towards a detailed understanding of magnesium ions on hydroxyapatite crystallization inhibition, Cryst. Growth Des., 14 (2014) 763–769.
[32] V.F.-C. Jose, L.-R. Roberto, M.-B. Jovita, M.G.-C. Rosa, A.-P. Antonio, J.L.-D. Gladis, Sorption mechanism of Cd(II) from water solution onto chicken eggshell, Appl. Surf. Sci., 276 (2013) 682–690.
[33] N. Liang, B. Min, G. Feng, Z. Zhu, Passivation remediation performance of lead-contaminated soil by hierarchical porous material of hydroxyapatite coated on bamboo biochar, J. Guilin Univ. Technol., 41 (2021) 193–200.
[34] M. Liang, D. Wang, Y. Zhu, Y. Xiao, Z. Zhu, S. Tang, Preparation of hydroxylapatite/bagasse biochar composite adsorbent and its adsorption mechanism on As(V) from aqueous solution, Res. Environ. Sci., 30 (2017) 607–614.
[35] Q. Zhang, F. Liu, A. Yang, J. Zhu, W. Yang, Adsorption characteristics and fixation effect of Mg-HAp on Mn in coal gangue, Ind. Water Treat., 41 (2021) 61–66.
[36] S. Teerakanok, M. Zhao, R. Giordano, Y. Fan, Interaction of doped magnesium, zinc and fluoride ions on hydroxyapatite crystals grown on etched human enamel, J. Cryst. Growth, 571 (2021) 126262, doi: 10.1016/j.jcrysgro.2021.126262.
[37] Y. Li, M.A. Taggart, C. McKenzie, Z. Zhang, Y. Lu, S. Pap, S. Gibb, Utilizing low-cost natural waste for the removal of pharmaceuticals from water: mechanisms, isotherms and kinetics at low concentrations, J. Cleaner Prod., 227 (2019) 88–97.
[38] A.I. Ivanets, V. Srivastava, N.V. Kitikova, I.L. Shashkova, M. Sillanpää, Kinetic and thermodynamic studies of the Co(II) and Ni(II) ions removal from aqueous solutions by Ca-Mg phosphates, Chemosphere, 171 (2017) 348–354.
[39] A.A. Attia, S.A. Khedr, S.A. Elkholy, Adsorption of chromium ion (VI) by acid activated carbon, Braz. J. Chem. Eng., 27 (2010) 183–193.
[40] Y. Zhou, W. Li, X. Jiang, Y. Sun, H. Yang, Q. Liu, Y. Cao, Y. Zhang, H. Cheng, Synthesis of strontium (Sr) doped hydroxyapatite (HAp) nanorods for enhanced adsorption of Cr(VI) ions from wastewater, Ceram. Int., 47 (2021) 16730–16736.
[41] F. Wang, W. Sun, W. Pan, N. Xu, Adsorption of sulfamethoxazole and 17β-estradiol by carbon nanotubes/$CoFe_2O_4$ composites, Chem. Eng. J., 274 (2015) 17–29.
[42] L. Bandura, M. Białoszewska, S. Malinowski, W. Franus, Adsorptive performance of fly ash-derived zeolite modified by β-cyclodextrin for ibuprofen, bisphenol A and caffeine removal from aqueous solutions – equilibrium and kinetic study, Appl. Surf. Sci., 562 (2021) 150160, doi: 10.1016/j.apsusc.2021.150160.
[43] M.M. Rao, A. Ramesh, G.P.C. Rao, K. Seshaiah, Removal of copper and cadmium from the aqueous solutions by activated carbon derived from *Ceiba pentandra* hulls, J. Hazard. Mater., 129 (2006) 123–129.
[44] W. Guo, X. Liang, D. Lin, Y. Xu, L. Wang, Y. Sun, X. Qin, Adsorption of Cd^{2+} on biochar from aqueous solution, Environ. Sci., 34 (2013) 3716–3721.
[45] Y. Xiao, Y. Xue, F. Gao, A. Mosa, Sorption of heavy metal ions onto crayfish shell biochar: effect of pyrolysis temperature, pH and ionic strength, J. Taiwan Inst. Chem. Eng., 80 (2017) 114–121.
[46] K. Kadirvelu, M. Kavipriya, C. Karthika, N. Vennilamani, S. Pattabhi, Mercury(II) adsorption by activated carbon made from sago waste, Carbon, 42 (2004) 745–752.
[47] K. Song, H. Huang, M. Lu, A. Yang, J. Weng, K. Duan, Hydrothermal preparation and characterization of Zn, Si, Mg, Fe doped hydroxyapatite, J. Inorg. Mater., 36 (2021) 1091–1096.
[48] Y.-Y. Wang, Y.-X. Liu, H.-H. Lu, R.-Q. Yang, S.-M. Yang, Competitive adsorption of Pb(II), Cu(II), and Zn(II) ions onto hydroxyapatite-biochar nanocomposite in aqueous solutions, J. Solid State Chem., 261 (2018) 53–61.
[49] Y.-Y. Wang, H.-H. Lu, Y.-X. Liu, S.-M. Yang, Removal of phosphate from aqueous solution by SiO_2-biochar nanocomposites prepared by pyrolysis of vermiculite treated algal biomass, RSC Adv., 6 (2016) 83534–83546.
[50] P.F. Zito, A. Caravella, A. Brunetti, E. Drioli, G. Barbieri, Estimation of Langmuir and Sips models adsorption parameters for NaX and NaY, J. Chem. Eng. Data, 60 (2015) 2858–2868.
[51] H. Cao, X. Wu, S.S.A. Syed-Hassan, S. Zhang, S.H. Mood, Y.J. Milan, M. Garcia-Perez, Characteristics and mechanisms of phosphorous adsorption by rape straw-derived biochar functionalized with calcium from eggshell, Bioresour. Technol., 318 (2020) 124063, doi: 10.1016/j.biortech.2020.124063.
[52] A.I. Ivanets, N.V. Kitikova, I.L. Shashkova, O.V. Oleksiienko, I. Levchuk, M. Sillanpää, Removal of Zn^{2+}, Fe^{2+}, Cu^{2+}, Pb^{2+}, Cd^{2+}, Ni^{2+} and Co^{2+} ions from aqueous solutions using modified phosphate dolomite, J. Environ. Chem. Eng., 2 (2014) 981–987.
[53] A.I. Ivanets, V. Srivastava, N.V. Kitikova, I.L. Shashkova, M. Sillanpää, Non-apatite Ca-Mg phosphate sorbent for removal of toxic metal ions from aqueous solutions, J. Environ. Chem. Eng., 5 (2017) 2010–2017.
[54] A.N. Amenaghawon, C.L. Anyalewechi, H. Darmokoesoemo, H.S. Kusuma, Hydroxyapatite-based adsorbents: applications in sequestering heavy metals and dyes, J. Environ. Manage., 302 (2022) 113989, doi: 10.1016/j.jenvman.2021.113989.
[55] L.P. Higuita, A.F. Vargas, M.J. Gil, L.F. Giraldo, Synthesis and characterization of nanocomposite based on hydroxyapatite and monetite, Mater. Lett., 175 (2016) 169–172.
[56] X. Cao, L.Q. Ma, D.R. Rhue, C.S. Appel, Mechanisms of lead, copper, and zinc retention by phosphate rock, Environ. Pollut., 131 (2004) 435–444.
[57] S.V. Dorozhkin, Amorphous calcium (ortho)phosphates, Acta Biomater., 6 (2010) 4457–4475.